Research Article | Vol. 7, No. 3 | 1 Mar 2017 | OPTICAL MATERIALS EXPRESS 2863

Optics EXPRESS

Coupling erbium dopants in yttrium orthosilicate to silicon photonic resonators and waveguides

EVAN MIYAZONO,[1,2] IOANA CRAICIU,[1,2] AMIR ARBABI,[1] TIAN ZHONG,[1] AND ANDREI FARAON[1,*]

[1]*T. J. Watson Laboratory of Applied Physics, California Institute of Technology, 1200 E California Blvd, Pasadena, CA, 91125, USA*

[2]*These authors contributed equally to this work*

[*]*faraon@caltech.edu*

Abstract: A scalable platform for on-chip optical quantum networks will rely on standard top-down nanofabrication techniques and solid-state emitters with long coherence times. We present a new hybrid platform that integrates amorphous silicon photonic waveguides and microresonators fabricated on top of a yttrium orthosilicate substrate doped with erbium ions. The quality factor of one such resonator was measured to exceed 100,000 and the ensemble cooperativity was measured to be 0.54. The resonator-coupled ions exhibited spontaneous emission rate enhancement and increased coupling to the input field, as required for further development of on-chip quantum light-matter interfaces.

OCIS codes: (130.3120) Integrated optics devices; (210.4810) Optical storage-recording materials; (220.4241) Nanostructure fabrication; (160.5690) Rare-earth-doped materials; (270.0270) Quantum optics; (020.5580) Quantum electrodynamics.

References and links

1. H. J. Kimble "The quantum internet," Nature **453**(7198), 1023–1030 (2008).
2. J. L. O'Brien, A. Furusawa, and J. Vučković "Photonic quantum technologies," Nat. Photon. **3**(12), 687–695 (2010).
3. T. E. Northup and R. Blatt "Quantum information transfer using photons," Nat. Photon. **8**(5), 356–363 (2014).
4. A. I. Lvovsky, B. C. Sanders, and W. Tittel "Optical quantum memory," Nat. Photon. **3**(12), 706–714 (2009).
5. F. Bussières, N. Sangouard, M. Afzelius, H. de Riedmatten, C. Simon, and W. Tittel "Prospective applications of optical quantum memories," J. Mod. Optics **60**(18), 1519–1537 (2013).
6. M. Zhong, M. P. Hedges, R. L. Ahlefeldt, J. G. Bartholomew, S. E. Beavan, S. M. Wittig, J. J. Longdell, and M. J. Sellars "Optically addressable nuclear spins in a solid with a six-hour coherence time," Nature **517**(7533), 177–180 (2015).
7. E. Saglamyurek, N. Sinclair, J. Jin, J. A. Slater, D. Oblak, F. Bussières, M. George, R. Ricken, W. Sohler, and W. Tittel "Broadband waveguide quantum memory for entangled photons," Nature **469**(7331), 512–515 (2011).
8. G. Corrielli, A. Seri, M. Mazzera, R. Osellame, and H. de Riedmatten "Integrated optical memory based on laser-written waveguides," Phys. Rev. Applied **5**(5), 054013 (2016).
9. T. Zhong, J. M. Kindem, E. Miyazono, and A. Faraon "Nanophotonic coherent light-matter interfaces based on rare-earth-doped crystals," Nature Commun. **6**, 8206 (2015).
10. S. Marzban, J. G. Bartholomew, S. Madden, K. Vu, and M. J Sellars "Observation of photon echoes from evanescently coupled rare-earth ions in a planar waveguide," Phys. Rev. Lett. **115**(1), 013601 (2015).
11. D. Ding, L. M. C. Pereira, J. F. Bauters, M. J. R. Heck, G. Welker, A. Vantomme, J. E. Bowers, M. J. A. de Dood, and D. Bouwmeester "Multidimensional Purcell effect in an ytterbium-doped ring resonator," Nat. Photon. **10**(6), 385–388 (2016).
12. D. L. McAuslan and J. J. Longdell "Strong-coupling cavity QED using rare-earth-metal-ion dopants in monolithic resonators: What you can do with a weak oscillator," Phys. Rev. A **80**(6), 062307 (2009).
13. D. McAuslan, D. Korystov, and J. Longdell "Coherent spectroscopy of rare-earth-metal-ion-doped whispering-gallery-mode resonators," Phys. Rev. A **83**(6), 063847 (2011).
14. T. Zhong, J. Rochman, J. M. Kindem, E. Miyazono, and A. Faraon "High quality factor nanophotonic resonators in bulk rare-earth doped crystals," Opt. Express **24**(1), 536 (2016).
15. T. Zhong, J. M. Kindem, J. Rochman, and A. Faraon "Interfacing broadband photonic qubits to on-chip cavity-protected rare-earth ensembles," Nature Commun. **8**, 14107 (2017).
16. M. Afzelius and C. Simon "Impedance-matched cavity quantum memory," Phys. Rev. A **82**(2), 022310 (2010).

#280222 https://doi.org/10.1364/OE.25.002863
Journal © 2017 Received 7 Nov 2016; revised 25 Jan 2017; accepted 26 Jan 2017; published 3 Feb 2017

Optics EXPRESS

17. E. Miyazono, T. Zhong, I. Craiciu, J. M. Kindem, and A. Faraon "Coupling of erbium dopants to yttrium orthosilicate photonic crystal cavities for on-chip optical quantum memories," Appl. Phys. Lett. **108**(1), 011111 (2016).
18. B. Lauritzen, S. R. Hastings-Simon, H. De Riedmatten, M. Afzelius, and N. Gisin "State preparation by optical pumping in erbium-doped solids using stimulated emission and spin mixing," Phys. Rev. A **78**(4), 043402 (2008).
19. T. Böttger, C. Thiel, R. Cone, and Y. Sun "Effects of magnetic field orientation on optical decoherence in Er^{3+}:Y_2SiO_5," Phys. Rev. B **79**(11), 115104 (2009).
20. M. Rančić, M. P. Hedges, R. L. Ahlefeldt, M. J. Sellars, "Coherence time of over a second in a telecom-compatible quantum memory storage material," http://arxiv.org/abs/1611.04315.
21. E. Saglamyurek, J. Jin, V. B Verma, M. D Shaw, F. Marsili, S. W. Nam, D. Oblak, and W. Tittel "Quantum storage of entangled telecom-wavelength photons in an erbium-doped optical fibre," Nat. Photon. **9**(2), 83–87 (2015).
22. V. Damon, M. Bonarota, A. Louchet-Chauvet, T. Chanelière, and J. L. Le Gouët "Revival of silenced echo and quantum memory for light," New J. Phys. **13**(9), 093031 (2011).
23. A. F. Oskooi, D. Roundy, M. Ibanescu, P. Bermel, J. D. Joannopoulos, and S. G. Johnson "Meep: A flexible free-software package for electromagnetic simulations by the FDTD method," Comput. Phys. Commun. **181**(3), 687–702 (2010).
24. T. Böttger, Y. Sun, C. Thiel, and R. Cone "Spectroscopy and dynamics of Er^{3+}:Y_2SiO_5 at 1.5μm," Phys. Rev. B **74**(7), 075107 (2006).
25. V. B. Verma, B. Korzh, F. Bussières, R. D. Horansky, A. E. Lita, F. Marsili, M. D. Shaw, H. Zbinden, R. P. Mirin, and S. W. Nam "High-efficiency WSi superconducting nanowire single-photon detectors operating at 2.5 K," Appl. Phys. Lett. **105**(12), 2013–2016 (2014).
26. S. Mosor, J. Hendrickson, B. C. Richards, J. Sweet, G. Khitrova, H. M. Gibbs, T. Yoshie, a. Scherer, O. B. Shchekin, and D. G. Deppe "Scanning a photonic crystal slab nanocavity by condensation of xenon," Appl. Phys. Lett. **87**(14), 141105 (2005).
27. I. Diniz, S. Portolan, R. Ferreira, J. M. Gérard, P. Bertet, and A. Auffèves "Strongly coupling a cavity to inhomogeneous ensembles of emitters: Potential for long-lived solid-state quantum memories," Phys. Rev. A **10**(6), 385–388 (2011).
28. P. E. Barclay, K. Fu, C. Santori, and R. G. Beausoleil "Hybrid photonic crystal cavity and waveguide for coupling to diamond NV-centers," Opt. Express **17**(12), 9588 (2009).
29. E. Waks and D. Sridharan "Cavity QED treatment of interactions between a metal nanoparticle and a dipole emitter," Phys. Rev. A **82**(4), 043845 (2010).
30. H. de Riedmatten, M. Afzelius, M. U. Staudt, C. Simon, and N. Gisin "A solid-state light-matter interface at the single-photon level," Nature **456**(7223), 773–777 (2008).
31. B. Kraus, W. Tittel, N. Gisin, M. Nilsson, S. Kröll, and J. I. Cirac "Quantum memory for nonstationary light fields based on controlled reversible inhomogeneous broadening," Phys. Rev. A **73**(2), 20302 (2006).
32. A. L. Alexander, J. J. Longdell, M. J. Sellars, and N. B. Manson "Photon echoes produced by switching electric fields," Phys. Rev. Lett. **96**(4), 043602 (2006).
33. S. R. Hastings-Simon, B. Lauritzen, M. U. Staudt, J. L. M. van Mechelen, C. Simon, H. de Riedmatten, M. Afzelius, and N. Gisin "Zeeman-level lifetimes in Er3+:Y2SiO5," Phys. Rev. B **78**(8), 085410 (2008).
34. B. Lauritzen, J. Minář, H. de Riedmatten, M. Afzelius, N. Sangouard, C. Simon, and N. Gisin "Telecommunication-wavelength solid-state memory at the single photon level," Phys. Rev. Lett. **104**(8), 080502 (2010).
35. R. E. Evans, A. Sipahigil, D. D. Sukachev, A. S. Zibrov, and M. D. Lukin "Narrow-linewidth homogeneous optical emitters in diamond nanostructures via silicon ion implantation," Phys. Rev. Applied **5**(4), 044010 (2016).
36. W. F. Koehl, B. B. Buckley, F. J. Heremans, G. Calusine, and D. D. Awschalom "Room temperature coherent control of defect spin qubits in silicon carbide," Nature **479**(7371), 84–87 (2011).

1. Introduction

A scalable on-chip method for routing and storing photonic quantum bits is an integral requirement for numerous quantum information processing technologies [1–3]. To date, the best solid-state optical quantum memories are based on rare-earth-doped materials [4–6]. Steps towards integrating rare-earth ensembles with on-chip waveguides have been taken using waveguides fabricated by ion implantation [7], laser-writing [8], and focused ion beam milling [9]. Hybrid platforms where the waveguides are fabricated in deposited layers of chalcogenide glasses [10] and silicon nitride [11] have also been explored. However, the most scalable on-chip photonic platform would harness the excellent prospects for integration provided by silicon photonics and likely leverage the coherence properties of rare earth host crystals. In this letter we take the first step towards integrating ensembles of erbium ions doped in yttrium orthosilicate with on-chip silicon resonators and waveguides.

Rare earth ions (REIs) make excellent quantum memory materials because of their long optical and spin coherence times [5]. Optical signals can be stored directly on the optical transition for

Optics EXPRESS

tens to hundreds of microseconds. By transferring to a spin wave, the storage time can be extended to milliseconds and possibly hours [6]. However, these long optical coherence times arise from a low oscillator strength, which results in weak interaction with control fields and photonic qubits. It has been shown in theory and experiment that optical resonators can increase the coupling strength between the optical field and the ions [12, 13]. Using small cavities [14] and large ensembles, the strong coupling regime can be reached [15]. Furthermore, impedance matching the input coupling rate of a cavity with negligible intrinsic loss to the collective absorption rate of the ions should engender optical memories with high efficiency [16]. Additionally, as we have shown previously [9, 17], excited state lifetime modification, which is necessary for efficient state initialization for memory protocols [18], can be achieved by coupling the transition to a resonant structure.

In this work, we experimentally demonstrate silicon waveguides and optical microresonators coupled to erbium dopants in single crystal yttrium orthosilicate (YSO). Utilizing a magnetically quiet, crystalline host like YSO is paramount if the narrow inhomogeneous linewidth and long coherence times of rare earth ions are to be utilized; the longest coherence time demonstrated so far for any qubit in solid state is a 6 hour coherence time for the hyperfine levels of europium in YSO [6]. Erbium was chosen among REIs because it possesses a long-lived and highly radiative transition corresponding to a wavelength in the most commonly used optical fiber transparency window, the telecommunications C band. In YSO, erbium has been shown to have optical coherence times longer than 4 ms [19] and hyperfine coherence times of isotopically pure erbium-167 doped YSO have been demonstrated to be longer than a second [20]. For comparison, in SiO_2 the optical coherence time for erbium ions has been measured to be on the order of 35 ns at ~1 K, while the optical inhomogeneous broadening, roughly 1.3 THz, is large in SiO_2 because it is not a crystalline host [21].

The silicon ring microresonators demonstrated in this work were fabricated on erbium doped YSO (Er:YSO) using standard nanofabrication techniques and have quality factors exceeding 100,000. The erbium ions were evanescently coupled to a waveguide-coupled mode of the ring resonators. Compared to 1D and 2D photonic crystal cavities, ring resonators support traveling wave modes, which interact with twice as many ions as the standing wave mode for the same mode volume. Furthermore, traveling modes in ring resonators can support phase-matching selective processes for protocols such as the Revival of Silenced Echo (ROSE) [22].

2. Device simulation

The microring was designed using the MIT Electromagnetic Equation Propagation (MEEP) software [23], optimizing dimensions for a first-order TM mode in the radial and axial directions. Axial and azimuthal cross sections of the ring mode are shown in Fig. 1(a) and 1(b). The TM mode was chosen due to the increased field strength at the location of the ions, illustrated in Fig. 1(b), resulting from the continuity of the electric displacement across a boundary, which enhances coupling to the ions. The crystal was oriented such that the D2 axis, which provides the largest dipole moment for the 1536 nm transition [24], was orthogonal to the substrate surface to maximize the inner product between the dipole moment and the polarization of the TM mode.

A higher resolution MEEP simulation of the ring was run in cylindrical coordinates for a more precise field distribution. From this, and taking into account the modulation by a sinusoidal envelope around the ring, the mode volume was calculated to be $V_{\text{mode}} = \frac{\int \epsilon |\vec{E}|^2 dV}{\max(\epsilon |\vec{E}|^2)} = 2.93\,\mu\text{m}^3$ where $\vec{E}$ is the electric field of the cavity mode, ϵ is the permittivity, and max() denotes the maximum value the argument takes. The field distribution in the YSO substrate was used in determining the coupling rates for ions at various locations, $g_{\text{ion}}(\vec{r})$. When calculating the total coupling strength, the field was taken to be azimuthally symmetric, as the period of the ≈195 THz light is negligible compared to all other timescales, and thus all ions in the same radial and

Optics EXPRESS

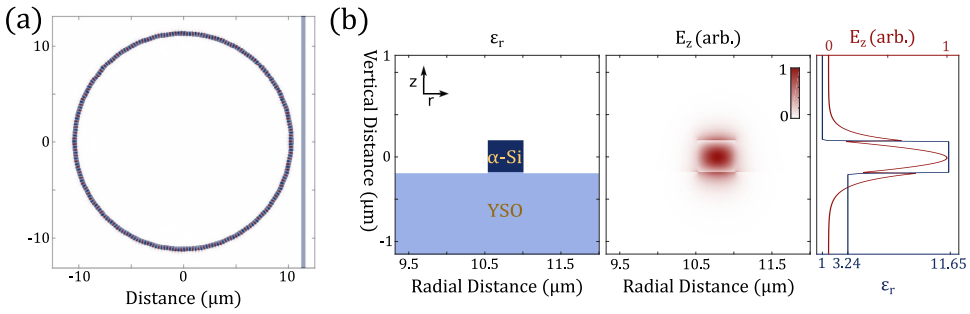

Fig. 1. (a) In-plane cross section of the ring resonator mode, with waveguide in light blue along the right. (b) *left:* Radial cross section of the amorphous silicon (α-Si) ring on erbium-doped YSO, showing the hybrid structure. The ring is 380 nm tall and 480 nm wide with an outer radius of 11.0 microns. *center:* the mode profile for the vertical component of the electric field. *right:* plot of the vertical component of the electric field and the relative permittivity as a function of the vertical displacement through the waveguide center.

axial position will experience the same time-averaged field strength.

3. Device fabrication

Optical resonators were fabricated using a scalable procedure, depicted in Fig. 2(a), which began with a Czochralski grown single crystal of YSO with 200 ppm erbium dopants obtained from Scientific Materials. A plasma enhanced chemical vapor deposition system was used to deposit 380 nm of amorphous silicon. Spin coating was used to apply first a 300 nm layer of ZEP520A electron beam resist, and then a layer of AquaSAVE-ZX to prevent charge accumulation. Electron beam lithography was then used to define the ring, waveguides, and couplers. After developing, the pattern was transferred into the amorphous silicon layer using a mixed mode etch of SF_6 and C_4F_8 in an inductively coupled plasma etching system. Lastly, the resist was stripped in heated Nano Remover PG (MicroChem).

A scanning electron micrograph of the completed device is shown in Fig. 2(b). The micrograph of the device depicts free-space light impinging on the input grating. This light is scattered into the waveguide and evanescently couples to the ring. The opposite end of the input waveguide is tapered to reduce back reflections, preventing spurious interference. A bend in the waveguides was used to implement polarization extinction between input and output light. Furthermore, a triangular feature between the two couplers is used to prevent scattering of light from the input coupler though the slab mode to the output grating coupler.

4. Characterization

Characterization of the sample was performed using a custom confocal microscope, diagrammed in Fig. 2(c). The sample was placed in a Janis ST-500 continuous flow liquid helium cryostat with no externally applied magnetic field and cooled to 4.5 K for the duration of the measurement. The excitation source used was a Toptica CTL external cavity diode laser (ECDL) tuned on resonance with the $^4I_{13/2}$ to $^4I_{15/2}$ transition of erbium ions. For scanning, the frequency of the laser was swept with a built in piezoelectric element. For lifetime measurements, the input was amplitude modulated by an acousto-optic modulator (AOM) before being directed through a beam splitter and objective onto the input coupler. The signal from the output coupler was spatially filtered using a telescope and a pinhole, and cross-polarized relative to the input. The output signal was coupled to a single-mode fiber with a lower numerical aperture than the pinhole to reduce spurious interference patterns arising from a non-negligible area on the grating coupler. The output was

Optics EXPRESS

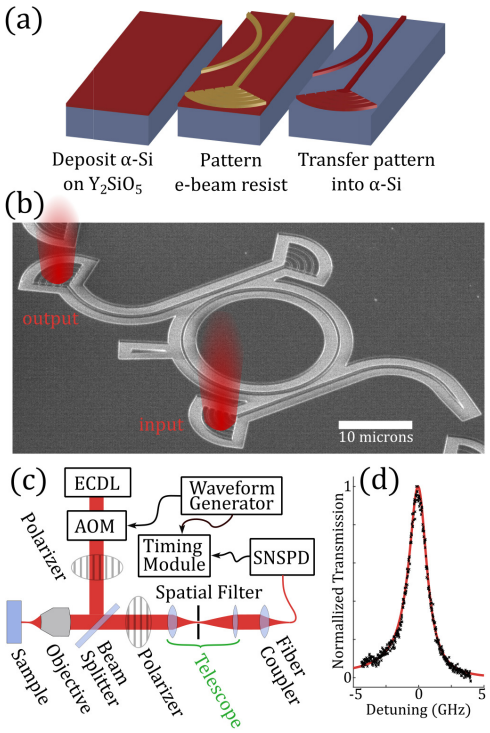

Fig. 2. (a) Hybrid fabrication procedure starts with the deposition of amorphous silicon, which is patterned via electron beam lithography and dry etching. (b) SEM micrograph of the completed device with input and output grating couplers, and laser beams sketched in as a visual aid. (c) Depiction of the confocal setup used to characterize the sample. (d) Transmission spectrum through the ring, fit with a Lorentzian curve illustrating 1.4 GHz linewidth, corresponding to a quality factor of 112,000.

measured with a tungsten silicide superconducting nanowire single photon detector [25] cooled to 480 mK in a BlueFors helium-3 fridge.

An electro-optic modulator and signal generator were used to add sidebands of known frequency in order to calibrate the piezo scan of laser frequency. This scan calibration was subsequently used to generate frequency scans of the resonator transmission. Fig. 2(d) shows the cavity transmission at 4.5 K, where the cavity FWHM is shown to be 1.4 GHz, which corresponds to a quality factor of 112,000. At room temperature, the quality factor of the same device was measured to be only 64,000; we believe thermally excited carriers provide an additional loss mechanism.

4.1. Characterization of coupling via transmission

Nitrogen gas was controllably bled into the cryostat so that the condensed nitrogen would coat the device, changing the mode's effective refractive index and shifting the resonance toward lower frequencies [26] through the frequency of the optical transition of interest. Between initial characterization and the completion of measurements, the quality factor degraded to a slightly lower value to be noted with later measurements. We believe the degradation was due to increased scattering or absorption by a combination of repeated nitrogen condensation and surface adsorption of atmospheric water vapors, as the quality factor could be recovered by heating to 200°C under vacuum. Scans of the tuning process are shown in Fig. 3(a). The scan

Optics EXPRESS

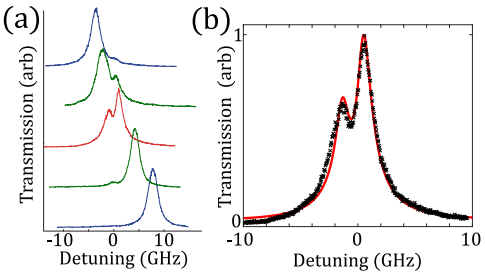

Fig. 3. (a) Multiple spectra showing the tuning procedure as gas is slowly let into the cryostat. The cavity transmission peak is seen moving through the ion absorption dip. (b) Transmission data compared to a simulation using a Lorentzian cavity resonance interacting with a Gaussian distribution of ions and a phase term to account for Fano interference from a spurious reflection. The simulation was fit for amplitude, detuning, and the Fano phase, using measured values for inhomogeneous broadening, and cavity linewidth, with the simulated total coupling rate.

shown in Fig. 3(b) was fit to the theoretical transmission for a cavity coupled to an ensemble of ions using

$$T = a\left|be^{i\phi} + \frac{-\frac{\kappa}{2}}{i(\omega-\omega_{\text{cavity}}) - \frac{\kappa}{2} - iW(\omega-\omega_{\text{ions}})}\right|^2, \tag{1}$$

for constants a and b where κ is the cavity energy decay rate, ϕ compensates for Fano interference between cavity transmission and a leakage mode, and

$$W(\omega) = -i\frac{\sqrt{\pi \ln 2}\,\Omega^2}{\Delta}\,\exp\left[\left(\frac{\omega+i\gamma/2}{\Delta/\sqrt{\ln 2}}\right)^2\right]\text{erfc}\left(-i\frac{\omega+i\gamma/2}{\Delta/\sqrt{\ln 2}}\right) \tag{2}$$

accounts for the coupling to an inhomogeneously broadened ensemble [27] that we assume is Gaussian distributed. In this expression $\Omega = \left[\int g_{\text{ion}}^2(\vec{r})\rho dV\right]^{1/2} = 0.537$ GHz is the ensemble coupling rate between the ions and the cavity from simulation, using the ion density, $\rho = 1.87$ million ions per cubic micron, and the position dependent coupling rate $g_{\text{ion}}(\vec{r})$, defined in Eq. (3). The atomic loss rate γ is much slower than all other rates and thus neglected, and $\Delta = 0.65$ GHz is the HWHM of the ensemble inhomogeneous broadening, measured in the bulk Er:YSO. The cavity energy decay rate $\kappa/2\pi = 2.43$ GHz, corresponding to a quality factor of Q = 80,400, was measured while the cavity was off-resonant. The ensemble cooperativity, defined as the ratio between the total absorption rate of the ions and the energy decay rate of the cavity when the two are coresonant, was computed to be $\eta = \frac{|W(0)|}{\kappa/2} = 0.54$. If Eqs. 1 and 2 are instead used to fit the data for the inhomogeneous linewidth, the resulting HWHM, $\Delta = 0.687$ GHz, shows little change from the bulk measured value of $\Delta = 0.65$ GHz, which indicates that processing does not substantially alter the crystal structure of the YSO.

4.2. *Characterization of coupling via lifetime modification*

To characterize the interaction of the cavity with the erbium ions, we performed a study of the optical transition lifetime of the ions as a function of detuning of the cavity resonance relative to the center of the inhomogeneous absorption line. It is expected that as the detuning decreases, the excited state decay rate increases via the Purcell effect, wherein the cavity mode provides an additional decay channel, and thus the optical lifetime of the ions decreases. To resonantly excite photoluminescence for various detunings, rectangular pulses 100 μs long were gated by the

Optics EXPRESS

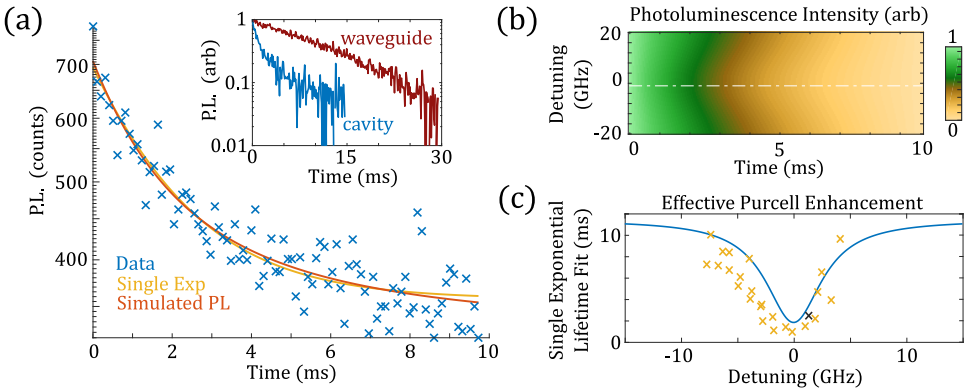

Fig. 4. (a) Photoluminescence (PL) decay from the cavity-coupled ions for a detuning of 1.13 GHz. Data has been fit using the simulated PL, scaled with a background, and a single exponential with a fitted lifetime, amplitude, and background. Inset shows normalized PL from ions coupled to a waveguide vs. ions coupled to the cavity. (b) Simulated PL as a function of time for a range of ion-cavity detunings. Detuning selected for subfigure (a) is highlighted as a dashed white line. (c) Single exponential lifetime fits from various detunings with a curve of lifetime vs. detuning generated using an averaged coupling strength across all ions. The black 'x' corresponds to the fit from (a).

AOM. At each detuning, the frequency of the cavity resonance transmission peak was measured on a Burleigh WA-1600 wavemeter and the photoluminescence (PL) decay curve was measured. A resonant PL curve is shown in the inset of Fig. 4(a), with a PL curve measured through a waveguide without a cavity for comparison. The waveguide excited state lifetime was found to be $T_1 = 11.4$ ms, in agreement with the bulk lifetime measured elsewhere [24].

In Fig. 4(a) we show the simulated PL curve for a detuning of 1.13 GHz, fitting only an amplitude coefficient and an offset. The expected PL curve was simulated by first calculating the expected coupling rate for ions in each simulated annulus pixel. This coupling is weighted by the electric field of the cavity mode at that ion, according to

$$g_{\text{ion}}(\vec{r}) = g_0 \left| \frac{E_z(\vec{r})}{\max(E_z)} \right| = \frac{\mu}{n_{\alpha\text{Si}}} \left[\frac{\omega}{2\hbar\epsilon_0 V_{\text{mode}}} \right]^{1/2} \left| \frac{E_z(\vec{r})}{\max(E_z)} \right|, \tag{3}$$

where $n_{\alpha\text{Si}} = 3.41$ is the refractive index of the amorphous silicon measured using ellipsometry and E_z is the field polarized perpendicular to the YSO surface [12, 28]. It was assumed that coupling to E_ϕ is negligible. To compute g_{ion}, the dipole moment $\mu = 2.07 \times 10^{-32}$ from [12] was used, as well as the simulated mode volume and field distribution. This was then used in a calculation of the Purcell enhanced total decay rate of each ion, according to $\Gamma_{\text{ion}} = \frac{1}{T_1} + \frac{\kappa g_{\text{ion}}^2}{(\kappa/2)^2 + \delta^2}$ where δ is the detuning between the ion and the cavity field [29], and T_1 is the bulk excited state lifetime. The contribution of each ion to the total PL is summed over the ensemble to generate the predicted PL for a given detuning. By simulating a range of detunings, a plot of predicted PL as a function of time was generated, and is shown in Fig. 4(b), with a horizontal dotted line indicating the detuning of the data in (a).

There is no simple analytic expression for the decay curve; because it is a sum of decays, each characterized by a Γ_{ion}, it therefore depends on an integral weighted by the distribution of the cavity mode profile in the YSO. Thus, to more clearly illustrate the effect, in Fig. 4(a) we include a single exponential curve that was fit for lifetime, amplitude, and background. Considered on a log plot, this is tantamount to approximating the PL curve, which is made up of a distribution of

Optics EXPRESS

many straight lines, as a single line. The deviation between the single exponential fit and the measured decay curves arises entirely from the non-uniform ion-cavity coupling, resulting from the variation in cavity field strength at the different locations of various ions. To extend the single exponential approximation, we calculate an effective coupling strength from the simulated field distribution by averaging the coupling of each ion, weighted by the coupling of that ion to the mode, as

$$\frac{g_{\text{eff}}}{2\pi} = \left[\frac{\int_{\text{YSO}} \left|E_z(\vec{r})\right|^2 \left(\frac{g_{\text{ion}}(\vec{r})}{(2\pi)}\right)^2 \rho \, dV}{\int_{\text{YSO}} \left|E_z(\vec{r})\right|^2 \rho \, dV}\right]^{1/2} = 0.211 \text{ MHz}, \tag{4}$$

where ρ is the density of ions per unit volume and the contribution of each ion is weighed by the proportion of the mode energy density at the ion, $\left|E_z(\vec{r})\right|^2$. This is necessary because the fraction of an ion's decay into the cavity mode, which is collected as PL, compared to the bulk, is proportional to the coupling strength between the cavity mode and that ion. We then approximate the single exponential decay rate as $\frac{1}{T_{\text{eff}}} = \frac{1}{T_1} + \frac{\kappa g_{\text{eff}}^2}{(\kappa/2)^2+\delta^2}$. From this simulated expected lifetime, we can extract an average Purcell factor at zero detuning of $T_1/T_{\text{eff}} - 1 = 5.25$.

The plot of the predicted effective lifetime as a function of detuning is shown in Fig. 4(c) along with the lifetimes extracted from single exponential fits of decay curves taken at various detunings. We draw attention to the fact that the lifetime of the optical transition continues to be affected by the presence of the cavity even when the detuning is many times the cavity linewidth. This difference is easily observed by comparison of Fig. 2(d) and 4(c). Specifically the half width at half maximum of the lifetime vs. detuning curve is approximately $\kappa\left[F_P\left(\frac{g_{\text{eff}}}{g_0}\right)^2 + 1\right]^{1/2}$, where $F_P = \frac{3}{4\pi^2}\beta Q\lambda^3/\left(V\chi_L n_{\alpha\text{Si}}^2 n_{\text{YSO}}\right)$ is the maximum Purcell factor [28]. Here χ_L accounts for the local correction to the dipole's field and $\beta = \frac{T_1}{T_{\text{spontaneous}}} = 0.21$ is the branching ratio of the 1536 nm decay, calculated using the dipole moment in [12].

5. Discussion and conclusion

The device presented here shows similar performance to our previous work coupling to erbium ensembles in highly coherent hosts [17]. Quantitatively, the quality factor to mode volume ratio and cooperativity for the triangular nanobeam cavities were $Q/\bar{V}_{\text{mode}} = 6900$ and $\eta = 0.48$, compared to the values $Q/\bar{V}_{\text{mode}} = 6600$ and $\eta = 0.54$ achieved in this work, where $\bar{V}_{\text{mode}}$ is the cavity mode volume normalized to the number of cubic wavelengths in the material. Despite a weaker cavity field at the ions' locations, the cooperativity of this device is slightly larger than that of the triangular nanobeam cavity because of the substantially higher quality factor. However, the significance of the results presented in this letter lies in the scalability fabrication method demonstrated.

In the context of quantum memories, the advantage of coupling an ensemble of erbium ions to a cavity is twofold. First, coupling an ensemble to a cavity has been predicted to drastically increase the recall efficiency of a quantum memory using a weak absorber [16]. Second, as we will outline here, the Purcell effect should ameliorate the notoriously difficult state initialization in Er:YSO [18], which is necessary for memory protocols that use spectral tailoring, such as atomic frequency combs [30] and controlled reversible inhomogeneous broadening (CRIB) [31, 32]. Spectral tailoring requires burning away population from one ground state into another auxiliary state, and the efficiency of this process is limited by the ratio between the decay rate from the excited state to the auxiliary state and the decay rate from the auxiliary state to the ground state, $\Gamma_{e\to aux}/\Gamma_{aux\to g}$. When a magnetic field is applied to Er:YSO, the unpaired electron spin of the erbium ion couples to the field, resulting in a ground state splitting that can be used together with an excited state as a lambda system. If the material is cooled to temperatures below 2 K, the

Optics EXPRESS

electron spin lifetime is on the order of hundreds of milliseconds [33]. However, due to the long optical state lifetime, the ratio $\Gamma_{e\rightarrow aux}/\Gamma_{aux\rightarrow g}$ is quite low, which is one of the few disadvantages of Er:YSO in quantum memory applications. While other methods have been proposed to remedy this including RF mixing and pumping on the excited state with a second laser [18], using a cavity would provide a simple solution requiring no additional inputs. In the cavity-ion system, one can set up the lambda system such that the memory transition is resonant with the cavity, and the decay to the auxiliary state is in the tails of the cavity but still experiences considerable Purcell enhancement due to the effect described above, such that $\Gamma_{e\rightarrow aux}/\Gamma_{aux\rightarrow g}$ is increased. This would lead to better state initialization and therefore higher memory efficiencies. While the quality factor of smaller rings is more sensitive to fabrication defects, if the ring diameter can be reduced, the reduced mode volume will increase the Purcell enhancement, thus improving the potential spectral tailoring efficiency.

Additionally, these devices can find broader applications beyond electron spin state manipulation. Similar devices on isotopically pure ^{167}Er:YSO could be used for spin-wave storage to provide a long-lived on demand optical quantum memory, or electrodes could be easily incorporated for a CRIB memory [34]. Alternatively, utilizing the second input coupler would allow for implementation of ROSE [22].

In summary, we have demonstrated evanescent coupling of an ensemble of erbium ions in a crystalline host to a silicon optical microresonator. The scalable nature of the silicon fabrication enables microscale optical quantum memories in the telecommunications C band that could be further integrated with other on-chip devices already developed for silicon photonics. Coupling the ensemble to a cavity has been predicted to increase the recall efficiency of a quantum memory using a weak absorber [16] and will improve the state initialization in Er:YSO [18]. Furthermore, this platform is transferable to an arbitrary substrate for coupling to interesting optical emitters in hosts that are not conducive to standard nanofabrication techniques, like diamond [35] and silicon carbide [36], provided the wavelength does not suffer from absorption in the amorphous silicon and the emitters' properties do not degrade within tens of nanometers from the surface.

Funding

Defense Advanced Research Projects Agency (DARPA) QUINESS W31P4Q-15-1-0012, AFOSR Young Investigator Award (FA9550-15-1-0252), Air Force Office of Scientific Research (AFOSR) Quantum Transduction MURI (FA9550-15-1-002). National Science Foundation (NSF) (PHY-1125565), Gordon and Betty Moore Foundation (GBMF-2644).

Acknowledgments

The authors would like to thank Y. Horie for discussions of fabrication techniques, J. Kindem and J. Bartholomew for discussions of REIs, Matt Shaw for the WSi SNSPD.